

Spectrum of Wave Forcing Associated with the Annual Cycle of Upwelling at the Tropical Tropopause

JOOWAN KIM

National Center for Atmospheric Research, Boulder, and Colorado State University,
Fort Collins, Colorado*

WILLIAM J. RANDEL

National Center for Atmospheric Research, Boulder, Colorado*

THOMAS BIRNER

Colorado State University, Fort Collins, Colorado

MARTA ABALOS

National Center for Atmospheric Research, Boulder, Colorado*

(Manuscript received 30 March 2015, in final form 11 November 2015)

ABSTRACT

The zonal wavenumber spectrum of atmospheric wave forcing in the lower stratosphere is examined to understand the annual cycle of upwelling at the tropical tropopause. Tropopause upwelling is derived based on the wave forcing computed from ERA-Interim using the momentum and mass conservation equations in the transformed Eulerian-mean framework. The calculated upwelling agrees well with other upwelling estimates and successfully captures the annual cycle, with a maximum during Northern Hemisphere (NH) winter. The spectrum of wave forcing reveals that the zonal wavenumber-3 component drives a large portion of the annual cycle in upwelling. The wave activity flux (Eliassen–Palm flux) shows that the associated waves originate from the NH extratropics and the Southern Hemisphere tropics during December–February, with both regions contributing significant wavenumber-3 fluxes. These wave fluxes are nearly absent during June–August. Wavenumbers 1 and 2 and synoptic-scale waves have a notable contribution to tropopause upwelling but have little influence on the annual cycle, except the wavenumber-4 component. The quasigeostrophic refractive index suggests that the NH extratropical wavenumber-3 component can enhance tropopause upwelling because these planetary-scale waves are largely trapped in the vertical, while being refracted toward the subtropical upper troposphere and lower stratosphere. Regression analysis based on interannual variability suggests that the wavenumber-3 waves are related to tropical convection and wave breaking along the subtropical jet in the NH extratropics.

1. Introduction

A strong annual cycle occurs in the mean upwelling circulation near the tropical tropopause, with approximately a factor-of-2 variation between boreal winter and

summer seasons. This climatological annual cycle of upwelling is an important feature that affects many physical and chemical properties of the tropical tropopause layer (TTL) and lower stratosphere and strongly modulates troposphere-to-stratosphere transport (Holton et al. 1995). In response to the upwelling, distinct annual cycles in temperature (Reed and Vleck 1969; Yulaeva et al. 1994; Fueglistaler et al. 2011) and water vapor (Mote et al. 1996; Randel and Jensen 2013) have been observed in the TTL and lower stratosphere. In general, strong upwelling is observed in the TTL during the Northern Hemisphere (NH) winter, leading to roughly 4–8-K colder and 1-ppmv drier TTL in the NH winter

*The National Center for Atmospheric Research is sponsored by the National Science Foundation.

Corresponding author address: Joowan Kim, National Center for Atmospheric Research, P.O. Box 3000, Boulder, CO 80307.
E-mail: joowan@ucar.edu

compared to the summer. In addition, tropical upwelling transports tropospheric air into the stratosphere, and thus an annual cycle is also found in the chemical composition of the tropical lower stratosphere for tracers with strong vertical gradients [e.g., in O_3 and CO (e.g., Schoeberl et al. 2006; Randel et al. 2008; Abalos et al. 2012; Stolarski et al. 2014)].

It is well known that tropical upwelling is a mechanically forced phenomenon (Haynes et al. 1991; Holton et al. 1995; Plumb and Eluszkiewicz 1999). Tropical upwelling is part of the global-scale stratospheric overturning circulation, which comprises ascent in the tropics and poleward and descending motion in the midlatitude and polar region [known as the Brewer–Dobson circulation (BDC); Brewer et al. 1949; Dobson 1956]. Recent work has highlighted that the BDC is composed of two branches: a deep branch driven by wave forcing in the deep stratosphere and a shallow branch driven by wave forcing in the subtropical and midlatitude lower stratosphere (Plumb 2002; Birner and Bönisch 2011). The deep branch is largely forced by planetary-scale waves that break in the extratropical (Garcia 1987; Yulaeva et al. 1994; Holton et al. 1995) and subtropical stratosphere (Plumb and Eluszkiewicz 1999; Ueyama et al. 2013), while the shallow branch is primarily forced by planetary and synoptic-scale waves that break in the subtropical lowermost stratosphere (Randel et al. 2008; Abalos et al. 2014). Although these two branches have similar driving mechanisms, the shallow branch is distinguished from the deep branch as it has more rapid circulation and confined vertical structure in the lower stratosphere (Birner and Bönisch 2011). Additionally, the upper and lower BDC branches behave independently on subseasonal time scales (Ueyama et al. 2013; Abalos et al. 2014; Randel and Wu 2015). The large annual cycle near the tropopause and lower stratosphere is associated primarily with the lower branch of the BDC.

However, despite the known links between wave forcing and tropical upwelling, the annual cycle in TTL upwelling is still poorly understood. It is clear that a seasonal difference in wave driving is the major mechanism of the annual cycle in upwelling, but the type and origin of the wave(s) that contributes to this seasonality are still unclear [see discussion in Fueglistaler et al. (2009)]. Yulaeva et al. (1994) and Holton et al. (1995) argued that the annual cycle could be explained by the deep BDC and the seasonal cycle in extratropical planetary-scale waves. This idea is supported by a strong negative correlation between time series of tropical and extratropical temperature in the lower stratosphere, which is observed from satellite measurements using Microwave Sounding Unit channel 4 (MSU-4; Yulaeva et al. 1994). However, Fueglistaler et al. (2011) revealed

that this strong correlation is partly a coincidence associated with the weighting function of the measurement. Plumb and Eluszkiewicz (1999) showed that low-frequency wave forcing needs to reach deep into the subtropics to force tropical upwelling. This led to an appreciation that wave dissipation in the subtropics associated with synoptic-scale waves could influence upwelling near the tropical tropopause (Randel et al. 2008; Taguchi 2009; Chen and Sun 2011; Jucker et al. 2013; Kim and Son 2015). Additionally, several recent studies have focused on the contribution of tropical planetary waves forced by deep convection to forced upwelling near the tropopause. Kerr-Munslow and Norton (2006), Norton (2006), and Ortland and Alexander (2014) emphasized the role of equatorial planetary-scale waves in the annual cycle using reanalysis and idealized global circulation model (GCM) experiments. Randel et al. (2008) explained the annual cycle as a combined result of enhanced tropical and extratropical waves in the NH winter using reanalysis data. They also suggested that both planetary and synoptic-scale waves are important for the extratropical wave forcing. Garny et al. (2011) also pointed out the importance of tropical and extratropical waves, but they focused more on the synoptic-scale waves for the extratropical component. Overall, there is no consensus on the waves that maintain the annual cycle in tropical upwelling.

Quantifying the sources of waves that drive the annual cycle is a crucial aspect for understanding variability in the TTL and related troposphere–stratosphere coupling processes. In this study, we revisit this problem to better understand the type and origin of the waves contributing to the annual cycle. Recent studies have shown that temperature variability near the tropical tropopause is largely independent from that in the deep stratosphere (e.g., Ueyama et al. 2013; Grise and Thompson 2013; Randel and Wu 2015); thus, we focus on wave forcing in the lower stratosphere, which directly induces the tropopause upwelling. The wave forcing is decomposed as a function of the zonal wavenumber in order to identify the scale and origin of the waves. We analyze the detailed structure of the wave forcing, including tropical and extratropical wave components, sources and propagation characteristics. Section 2 describes data and methodology. The results are presented in section 3 and summarized in section 4.

2. Data and methodology

a. ERA-Interim and NOAA OLR data

Wave forcing and upwelling are computed at every 6 h using temperature and wind from the European Centre for Medium-Range Weather Forecasts (ECMWF)

interim reanalysis (ERA-Interim; ECMWF 2009; Dee et al. 2011) archived in pressure coordinates. Daily and monthly means are obtained by averaging the 6-hourly calculation. Vertical resolution of the data is roughly 25 hPa near the TTL (levels are 150, 125, 100, 70, and 50 hPa), and data up to 10 hPa are used for the upwelling calculation. We use N128 Gaussian grid data (512 × 256 grid points in longitude and latitude) with a horizontal resolution of about 0.7°. The climatologies shown in this study are based on the period of 1979–2012 (34 yr). Monthly National Oceanic and Atmospheric Administration (NOAA) outgoing longwave radiation (OLR; Liebmann and Smith 1996) is also used to understand the relationship between wave forcing and convective activity in the tropics.

b. Upwelling calculation

Upwelling is computed in terms of the transformed Eulerian-mean (TEM) residual vertical velocity. The TEM vertical velocity in spherical log-pressure coordinates (Andrews et al. 1987) is

$$\overline{w}^* \equiv \overline{w} + \frac{1}{a \cos \phi} \frac{\partial}{\partial \phi} \left(\cos \phi \frac{\overline{v'\theta'}}{\overline{\theta}_z} \right), \quad (1)$$

where an overbar represents zonal mean, a prime is the perturbation from the zonal mean.; w is vertical velocity, v is meridional velocity, and θ is potential temperature. The vertical coordinate is defined as $z \equiv -H \ln(p/p_0)$ with scale height $H = 7$ km and surface pressure $p_0 = 1000$ hPa.

There are significant uncertainties in \overline{w} from re-analyses, as they are a poorly constrained quantity in current data assimilation systems (e.g., Iwasaki 2009; Abalos et al. 2015). Zonal-mean upwelling can also be estimated using the momentum or thermodynamic energy equation (e.g., Abalos et al. 2012) instead of directly computing it from the definition [Eq.(1)]. For the momentum-based upwelling, we use the TEM momentum and mass conservation equations as in Randel et al. (2002). Following Randel et al. (2002), the mean upwelling averaged over a given latitude band (ϕ_1, ϕ_2) can be expressed as

$$\langle \overline{w}_m^* \rangle(z) = \frac{1}{\rho_0 a \int_{\phi_1}^{\phi_2} \cos \phi d\phi} \left\{ \int_z^{\infty} \frac{\rho_0(z') \cos \phi}{\hat{f}(\phi, z')} [\overline{u}_t(\phi, z') - \mathbf{DF}(\phi, z')] dz' \right\}_{\phi_1}^{\phi_2}, \quad (2)$$

where a is the radius of Earth (6371 km), $\rho_0 = \rho_s e^{-z/H}$ with constant density at the surface ρ_s , and $\hat{f}[\equiv f - (\overline{u} \cos \phi)_\phi / (a \cos \phi)]$ is absolute vorticity with background zonal wind \overline{u} . \mathbf{DF} is the divergence of the Eliassen–Palm flux \mathbf{F} scaled as

$$\mathbf{DF} = \frac{1}{\rho_0 a \cos \phi} \nabla \cdot \mathbf{F}, \quad (3)$$

with

$$\mathbf{F} = \rho_0 a \cos \phi (-\overline{v'u'} + \overline{u}_z \overline{v'\theta'/\theta_z}, \hat{f} \overline{v'\theta'/\theta_z} - \overline{w'u'}). \quad (4)$$

The momentum-based estimate is based on the zonal-mean momentum equation, in which wave drag (\mathbf{DF}) is balanced by the Coriolis torque of a poleward motion and zonal wind tendencies; the poleward motion is estimated using the momentum balance, and then upwelling is computed from the estimated poleward motion using mass continuity [leading to Eq. (2)]. Under steady-state conditions ($\overline{u}_t = 0$) the equation simplifies to the downward control result of Haynes et al. (1991). In this study, we focus on upwelling over the deep tropics (15°S–15°N; the actual latitude boundary is about 15.1°N/S because we use the ERA-Interim on an N128

Gaussian grid instead of an interpolated one; this is referred to as 15° for simplicity). Vertical integration is made from 0 to 100 hPa using the method described in Trenberth (1991). Six pressure levels (10, 20, 30, 50, 70, and 100 hPa) are used for the integration. We note that the \overline{u}_t term is mainly important in Eq. (2) for sub-seasonal time scales (Abalos et al. 2014), and for monthly or longer time scales, upwelling can be estimated accurately using only \mathbf{DF} , which is denoted as $\langle \overline{w}_{\mathbf{DF}}^* \rangle$ here. Here, parameterized gravity wave drag is not included as it has a negligible effect on upwelling in the deep tropics (15°S–15°N; Randel et al. 2008). We use $\langle \overline{w}_{\mathbf{DF}}^* \rangle$ as the main estimate of upwelling in the following analyses.

Another estimate of upwelling uses the TEM thermodynamic energy equation:

$$\frac{\partial \overline{\theta}}{\partial t} + \frac{1}{a} \frac{\partial \overline{\theta}}{\partial \phi} \overline{v}^* + \frac{\partial \overline{\theta}}{\partial z} \overline{w}^* + \frac{1}{\rho_0} \frac{\partial}{\partial z} [\rho_0 (\overline{\theta}_\phi \overline{v'\theta'/a\theta_z} + \overline{w'\theta'})] = \overline{Q}, \quad (5)$$

where \overline{Q} is zonal-mean diabatic heating rate in terms of potential temperature. The eddy transport term [last term on the left-hand side in Eq.(5)] can be neglected for

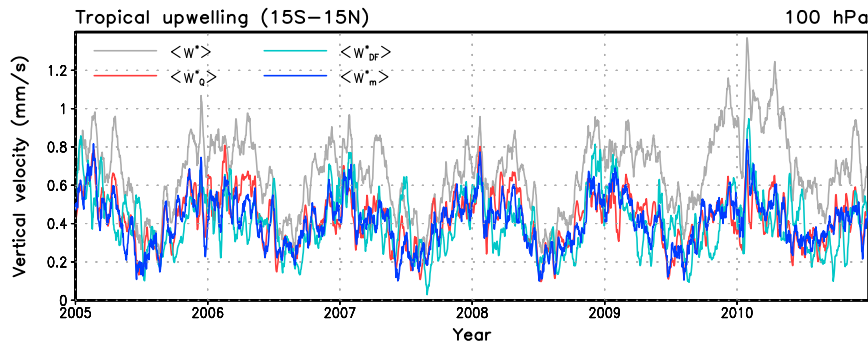


FIG. 1. Estimates of daily upwelling over 15°S–15°N based on thermodynamic balance ($\langle \bar{w}_Q^* \rangle$; red curve), momentum balance with **DF** ($\langle \bar{w}_{DF}^* \rangle$; light blue curve), and momentum balance with **DF** and \bar{u}_l ($\langle \bar{w}_m^* \rangle$; blue curve). The transformed Eulerian-mean residual vertical velocity computed from the definition ($\langle \bar{w}^* \rangle$; gray curve) is also shown. The 11-day running mean is applied for visual clarity.

small-amplitude waves, and with accurate values of \bar{Q} and $\bar{\theta}$, we can compute residual vertical velocity by iteratively solving the equation with the mass conservation equation until the values \bar{v}^* and \bar{w}^* converge (e.g., Gille et al. 1987; Rosenlof 1995; Abalos et al. 2012). The resulting vertical velocity is referred to as \bar{w}_Q^* . Because radiation is the primary source of diabatic heating near the tropopause, \bar{Q} can be estimated using radiative heating calculation. We compute \bar{Q} using the National Center for Atmospheric Research (NCAR) Column Radiation Model (CRM; Kiehl et al. 1996) along with daily ERA-Interim temperature and Microwave Limb Sounder (MLS) ozone data. Cloud radiative effect is not considered for the computation, as its influence is relatively small at the 100-hPa level (e.g., Yang et al. 2010). The detailed procedure can be found in Abalos et al. (2012). Our primary use of \bar{w}_Q^* is for comparison and validation of the momentum-based estimates.

c. Spectral decomposition of wave forcing

The zonal-mean wave forcing (**DF**) depends on zonal covariances of winds and temperatures [Eq. (4)], and these can be decomposed into components from individual zonal wavenumbers k using Fourier decomposition. Temperature and wind perturbations are decomposed by zonal wavenumber, and the Eliassen–Palm (EP) flux is computed for each wavenumber component. Hence, the total wave forcing (**DF**) can be expressed as the sum of the wave forcings from each wavenumber:

$$\mathbf{DF} = \sum_{k=1}^{\infty} \mathbf{DF}_k, \quad (6)$$

where subscript k is a zonal wavenumber. This decomposition helps to examine the scale of the dominant wave forcing and their propagation characteristics (e.g., Matsuno 1970).

3. Results

The analyses in this paper focus on the annual cycle of wave activity and the associated forcing in the subtropical lower stratosphere. Tropical upwelling is first computed and analyzed using Eq. (2); then the spectrum of the wave forcing is examined in detail. Finally, the sources and propagation characteristics of the waves that are responsible for the annual cycle are discussed.

a. Annual cycle of upwelling

Figure 1 presents the momentum-based estimates $\langle \bar{w}_m^* \rangle$ and $\langle \bar{w}_{DF}^* \rangle$ along with the thermodynamic-based estimate $\langle \bar{w}_Q^* \rangle$ and upwelling directly computed using Eq. (1) $\langle \bar{w}^* \rangle$ at 100 hPa. All the upwelling estimates show a distinct annual cycle with strong intraseasonal variabilities. Although nonnegligible differences are found between $\langle \bar{w}^* \rangle$ and the other estimates, all the calculations show a maximum in the NH winter and a minimum in the NH summer, which is consistent with the annual cycles reported in previous literature (e.g., Abalos et al. 2012). In particular, the two different upwelling estimates $\langle \bar{w}_m^* \rangle$ and $\langle \bar{w}_Q^* \rangle$ agree remarkably well. This agreement is encouraging because they are based on independent concepts (momentum balance versus thermodynamic energy balance). This suggests that these two are reliable estimates for 100-hPa upwelling. The momentum-based estimate using only wave forcing $\langle \bar{w}_{DF}^* \rangle$ also shows good agreement with the other two estimates, and in particular captures almost all of the seasonal variation. Figure 1 demonstrates that $\langle \bar{w}_{DF}^* \rangle$ is a good estimate for upwelling on monthly time scales.

It is worth noting that Fig. 1 shows that $\langle \bar{w} \rangle$ is generally larger than the other estimates, although their seasonal and subseasonal variability are quite similar. This discrepancy is also reported in the previous studies [Randel et al. (2008); Abalos et al. (2012) for ERA-Interim], and

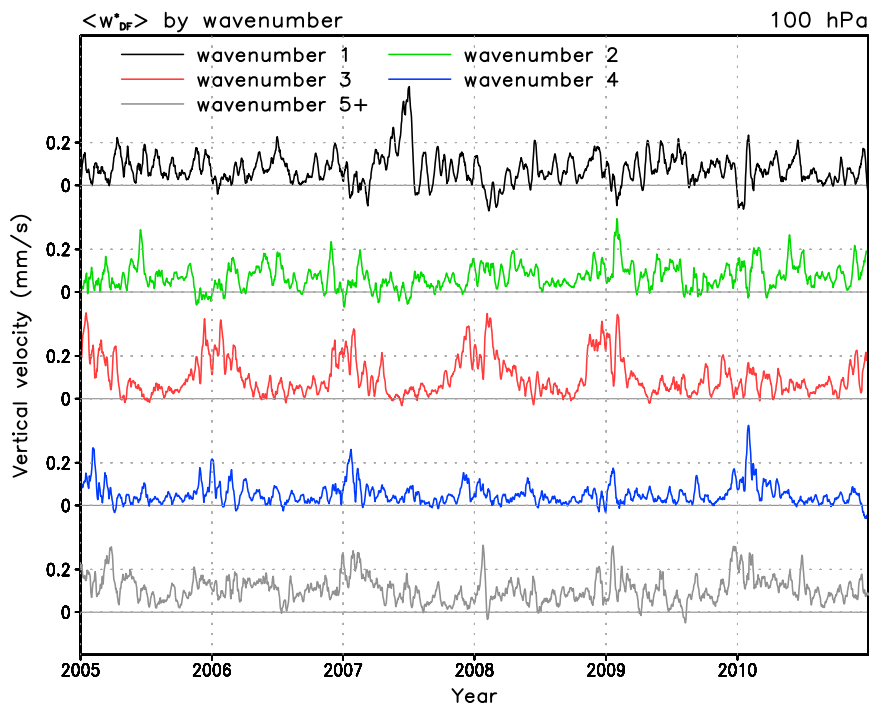


FIG. 2. Daily $\langle \bar{w}_{DF}^* \rangle$ as in Fig. 1, but for each zonal wavenumber.

it likely originates from vertical velocity \bar{w} of the re-analysis data, which is noisy and poorly constrained at the 100-hPa level. In the tropics, the TEM residual vertical velocity \bar{w}^* is largely determined by \bar{w} as the eddy heat flux term is small; thus, errors in \bar{w} can be pronounced in \bar{w}^* .

To understand the scale of wave forcing that contributes to the annual cycle, $\langle \bar{w}_{DF}^* \rangle$ is decomposed by

zonal wavenumber of DF. Figure 2 shows the time series of upwelling computed using the decomposed wave forcings. Interestingly, the decomposition reveals a clear annual cycle only in upwelling by the wavenumber-3 component ($\langle \bar{w}_{DF_3}^* \rangle$). Upwelling time series driven by other planetary-scale waves ($k = 1$ and 2) show large fluctuations in time but show no consistent annual cycle. Although wavenumber-4 upwelling exhibits an intermittent

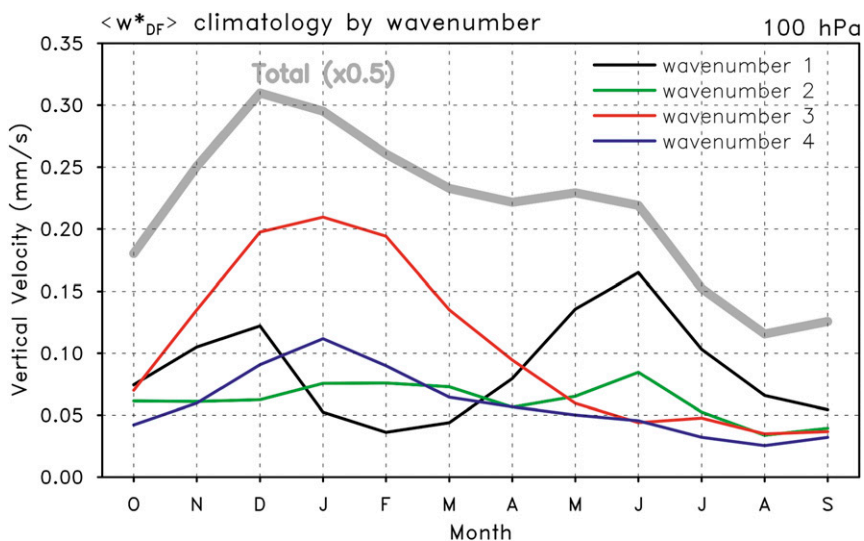


FIG. 3. Monthly climatology (1979–2012) of $\langle \bar{w}_{DF}^* \rangle$ for each zonal wavenumber ($k = 1-4$). Total upwelling is also shown in the thick gray curve (scaled by 0.5).

annual cycle, its amplitude is generally smaller than that of wavenumber 3. Higher wavenumbers ($k \geq 5$) essentially do not contribute to seasonal variability. The climatology of monthly mean upwelling for 1979–2012 (Fig. 3) confirms that the observed annual cycle is mostly explained by wavenumber 3. This result is surprising because the planetary-scale waves ($k = 1$ –3) originate from similar sources (Held 1983), and $k = 1$ and 2 waves are considered as potential contributors for the annual cycle. Upwelling forced by wavenumber 1 shows a semiannual cycle that has two peaks at December and June. Figure 4a summarizes the contribution of each wavenumber component in December–February (DJF) and June–August (JJA) upwelling. A large difference between DJF and JJA is found at wavenumber 3 with a secondary contribution from wavenumber 4. The wavenumber-4 contribution originates largely from the Southern Hemisphere and is likely related to transient waves, as shown in Randel et al. (2008). For a wider latitude band (e.g., Fig. 4b for 20°S–20°N and Fig. 4c for the turn-around latitudes), the $k = 3$ peak in DJF is gradually flattened along with a weakened annual cycle. However, $k = 3$ forcing still has a major contribution on the annual cycle. Note that the tropical band defined by the turn-around latitudes is wider in JJA ($\sim 18^\circ\text{S}$ – 41°N) than in DJF ($\sim 23^\circ\text{S}$ – 20°N). The weak JJA upwelling in Fig. 4c is partly due to the wide tropical band, which includes a weak upwelling area in the Northern Hemisphere.

b. Zonal wavenumber spectrum of wave forcing

To characterize the behavior of upwelling, the zonal spectrum of wave forcing (**DF**) at 100 hPa is examined as a function of latitude in Fig. 5. The **DF** spectrum in DJF (Fig. 5a) shows a pronounced forcing in the NH subtropics ($\sim 10^\circ$ – 20°N) at $k = 3$ and a secondary maximum in the SH subtropics ($\sim 10^\circ$ – 30°S) over a broader range of wavenumbers ($k = 2$ –4). These forcings are mostly absent in JJA (Fig. 5d), indicating that the forcings are responsible for the annual cycle. Further decomposition of the **DF** spectrum into horizontal (Figs. 5b,e) and vertical components (Figs. 5c,f) reveals that the strong NH forcing at $k = 3$ is largely as a result of horizontal convergence of waves propagating both from the tropics and extratropics (Fig. 5b). Strong poleward EP flux from the tropics and equatorward EP flux from the extratropics converge near 15°N and produce a large momentum forcing at $k = 1$ –3. This is very similar to the momentum flux (proportional to the horizontal EP flux) reported in Randel et al. (2008). However, the horizontal EP-flux convergence is largely cancelled by its vertical divergence for $k = 1$ and 2 (Fig. 5c), and therefore only $k = 3$ forcing dominates the

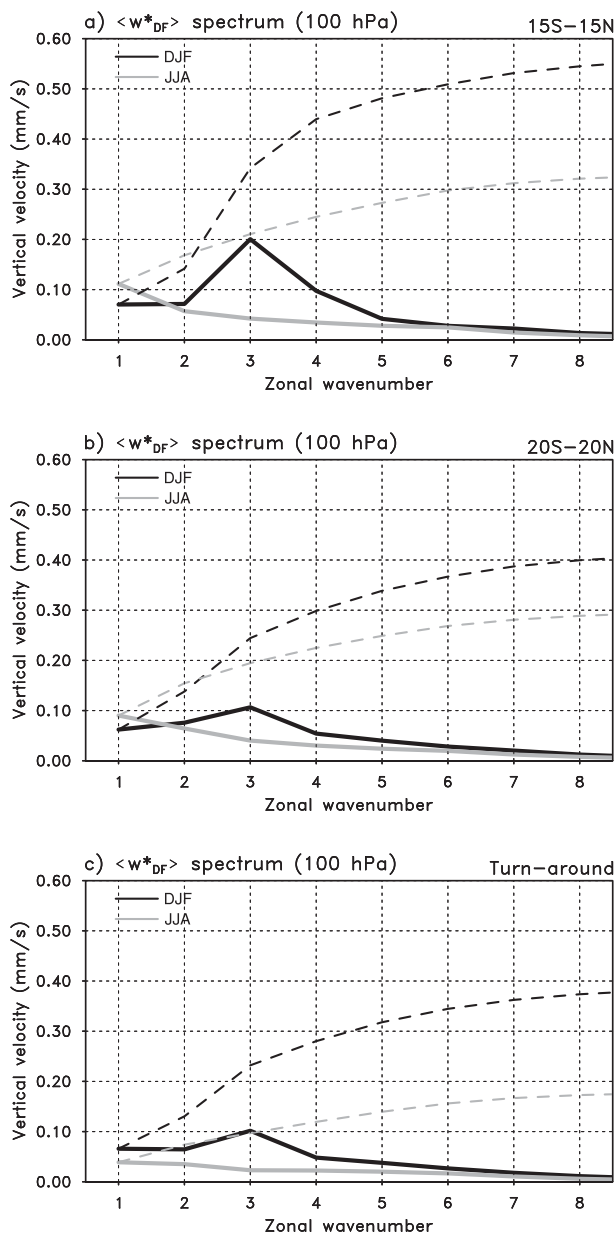


FIG. 4. December–February (black) and June–August (gray) climatologies (1979–2012) of $\langle \bar{w}_{\text{DF}}^* \rangle$ computed for (a) 15°S – 15°N , (b) 20°S – 20°N , and (c) the turn-around latitude as a function of wavenumber. Accumulated values are also shown (dashed curves). The monthly climatology of 100-hPa \bar{w}^* is used to determine the turn-around latitude.

DF spectrum in DJF. A similar behavior is also found at 70 hPa (not shown), except that extratropical waves dominate the forcing spectrum (the EP flux from the tropics is negligibly small at 70 hPa).

The wave forcing in the SH subtropics is dominated by vertical convergence of EP flux (Fig. 5c). This maximum is related to the horizontal heat flux $\overline{v'\theta'}$, and the latitude–height structure of EP fluxes (shown below)

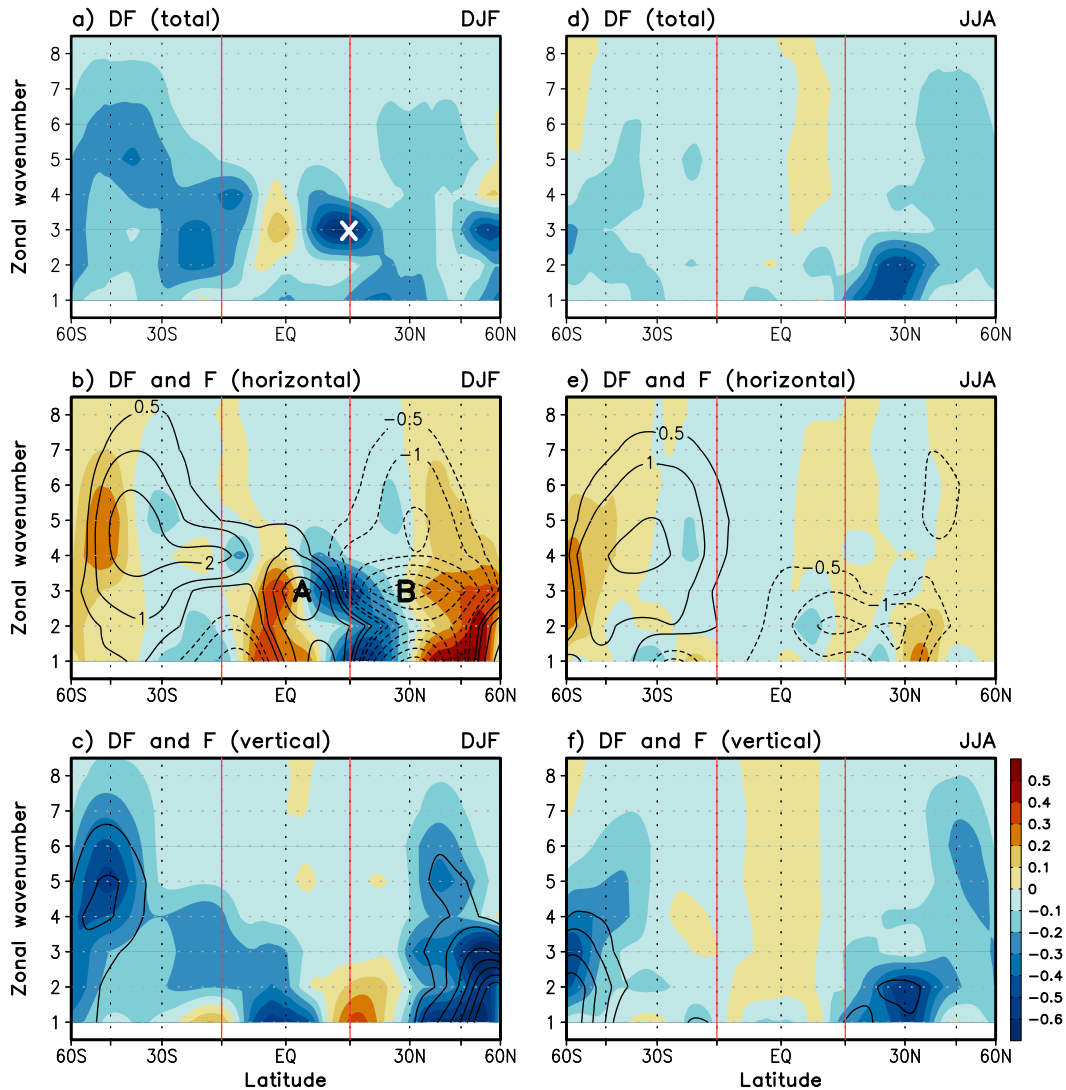


FIG. 5. Zonal wavenumber spectra of \mathbf{DF} ($\text{m s}^{-1} \text{ day}^{-1}$) at 100 hPa in (a)–(c) December–February and (d)–(f) June–August. The \mathbf{DF} computed from (a),(d) total; (b),(e) horizontal; and (c),(f) vertical EP flux components are shaded. (b),(e) The horizontal (10^6 kg s^{-2}) and (c),(f) vertical EP fluxes (10^4 kg s^{-2}) are also shown (counter interval is 1, and ± 0.5 contours are also shown). The letters A and B indicate the maximum and minimum of the horizontal EP flux at $k = 3$, which are found at 3.8° and 29.1°N , respectively.

implies that its source is located in the SH tropics and is likely related to convectively driven Rossby waves. This feature is similar to the result in Kerr-Munslow and Norton (2006), which emphasizes the role of vertical EP flux due to equatorial Rossby waves in the annual cycle, although the magnitude of this component is too weak to explain the observed annual cycle. This forcing is relatively shallow and almost absent in the 70-hPa spectrum (not shown). It is also worth noting that a similar wave forcing is found in JJA near 25°N (Fig. 5d), associated with vertical convergence of EP flux from $k = 1$ and 2 (Fig. 5f). In this region, the $k = 1$ forcing extends to 15°N and contributes to the strong June maximum in $k = 1$

upwelling (black curve in Fig. 3); thus, a semiannual cycle is produced for $k = 1$. The wave forcing possibly originates from deep convection in the Indian summer monsoon.

We further examine the spatial structure of the wavenumber-3 EP flux that is related to the annual cycle in upwelling. Figure 6 shows seasonal differences (DJF minus JJA) in $k = 3$ EP flux and \mathbf{DF} over the entire 1979–2012 record. As expected from the previous result (Fig. 5), the seasonal difference in \mathbf{DF} shows a strong forcing (negative \mathbf{DF}) near 100 hPa in the NH subtropics and a weaker maximum in the SH subtropics. The most pronounced feature in the EP-flux difference is a

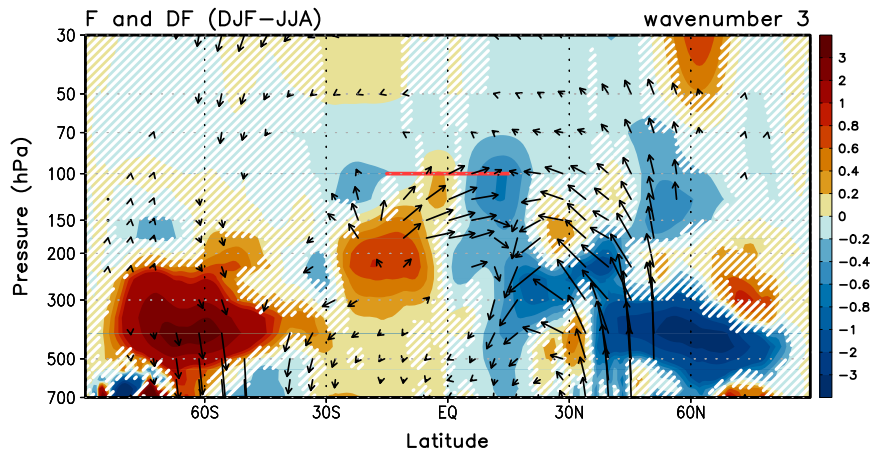


FIG. 6. Differences in $k = 3$ EP flux (vectors) and \mathbf{DF} ($\text{m s}^{-1} \text{ day}^{-1}$; shading) between DJF and JJA. Insignificant \mathbf{DF} difference is hatched in white, and only significant EP flux is shown (based on a Student's t test at the 99% confidence level). EP flux vectors are weighted in height by multiplying by $e^{z/H}$ for visual clarity.

convergence of two branches of wave activity propagating from the NH extratropics and SH tropics. In the SH tropics, there is a region of positive EP-flux divergence centered near 200 hPa, which is a signature of a source of wave activity likely associated with persistent deep convection (e.g., Dima et al. 2005). The two branches of $k = 3$ EP fluxes converge in the NH subtropics ($\sim 15^\circ\text{N}$) and produce the strong wave forcing over approximately 70–200 hPa. The magnitude of the tropical and extratropical wave fluxes is qualitatively similar at 100 hPa, suggesting that both components are important for the annual cycle in the TTL upwelling. Note that the seasonal differences in EP flux and \mathbf{DF} observed in the tropics are qualitatively similar to those of DJF climatology, because tropical $k = 3$ forcing is relatively weak in JJA.

It is worth noting that the subtropical wave forcing below 100 hPa may affect vertical motion at 100 hPa as a part of the transient response, which is observed on subseasonal time scales (e.g., Grise and Thompson 2013; Abalos et al. 2014). However, on seasonal or longer time scales, which could be assumed as steady state ($\bar{u}_t = 0$), only the forcing above 100 hPa affects upwelling at 100 hPa (Haynes et al. 1991).

c. Propagation and potential sources of wavenumber-3 waves

All extratropical planetary-scale waves (wavenumbers 1–3) exhibit maximum amplitudes in the troposphere during NH winter. Why is the wavenumber-3 contribution so dominant to the annual cycle of tropical upwelling? The extratropical EP fluxes in the NH (Fig. 6) provide a hint for this question. The $k = 3$ waves originating from the midlatitudes are refracted mostly

toward the subtropics while they propagate upward, with relatively little vertical transport to the stratosphere. Although they are attenuated significantly while traveling in the troposphere, still a good portion of the waves propagate into the subtropical upper troposphere–lower stratosphere (UTLS). This is a general feature of the extratropical $k = 3$ waves during DJF (note that they are almost absent in JJA; refer to Fig. 5).

This behavior is quite different from that of planetary-scale waves with $k = 1$ and 2. The $k = 1$ and 2 waves are typically not trapped in the UTLS but often propagate into the deep stratosphere during DJF. This feature can be understood from the quasigeostrophic (QG) refractive index. By assuming small-amplitude linear wave and constant buoyancy frequency N in the QG potential vorticity equation, the refractive index for stationary waves (Matsuno 1970) can be expressed as

$$n_k^2 = \frac{\bar{q}_\phi}{a\bar{u}} - \frac{f^2}{4H^2N^2} - \frac{k^2}{a^2 \cos^2\phi}, \quad (7)$$

where \bar{q} is the QG potential vorticity of zonal-mean state, and k is again zonal wavenumber. The refractive index describes direction of wave propagation: waves refract toward larger n_k^2 , and they are evanescent in the region of negative n_k^2 . Figure 7 shows the squared QG refractive index for $k = 1$ –4, along with climatological EP-flux vectors. As shown in previous literature (Matsuno 1970; Andrews et al. 1987, and references therein), a large portion of the $k = 1$ and 2 components propagate into the deep stratosphere in the extratropics. On the contrary, the $k = 3$ component is mostly trapped in the UTLS region and propagates toward subtropical latitudes (Fig. 7c). This behavior is consistent with

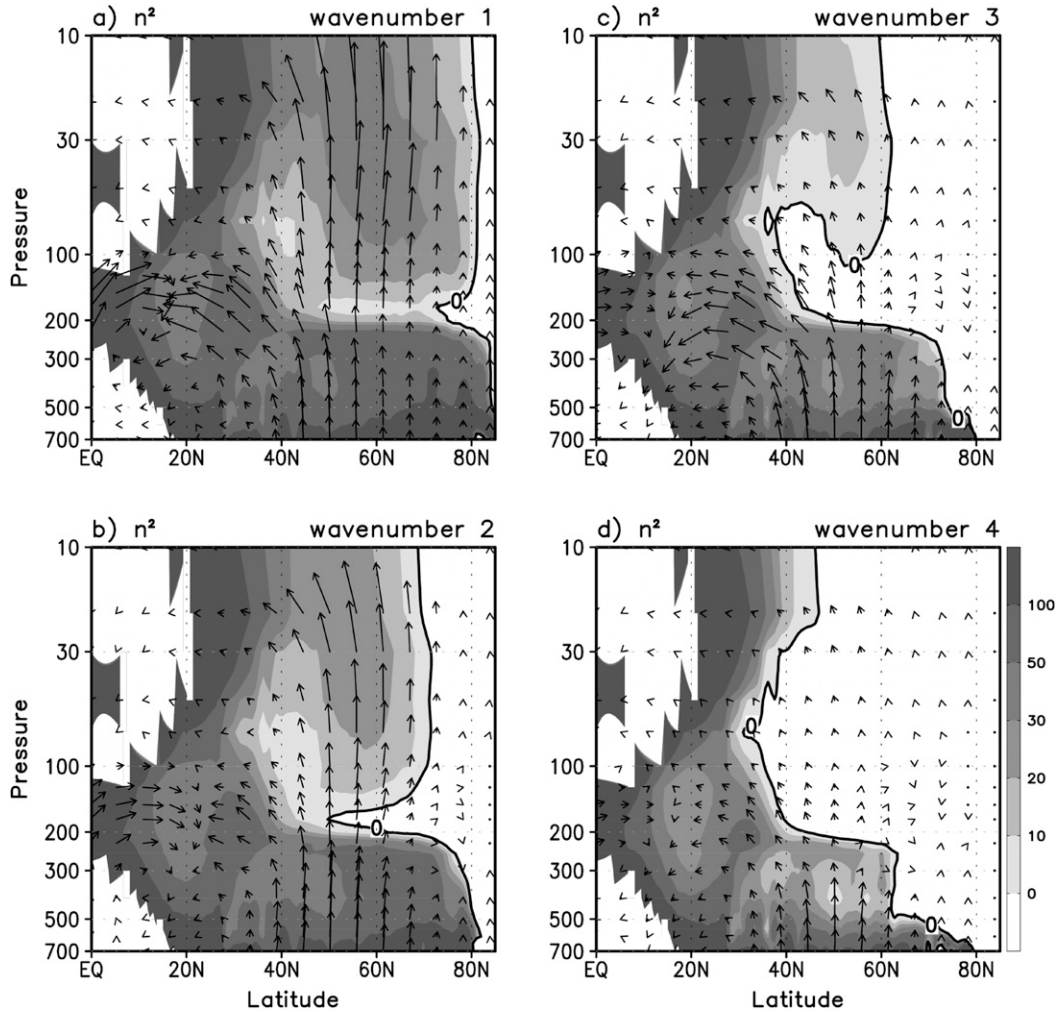


FIG. 7. Refractive index squared (shading) and EP flux climatology (vectors) for each wavenumber ($k = 1-4$) during DJF. Refractive indices are computed from DJF zonal wind climatology (1979–2012). EP flux vectors are weighted in height by multiplying by $e^{z/H}$ for visual clarity.

wavenumber-3 refractive index n_3^2 . A negative n_3^2 region, where waves cannot propagate, occurs above 200 hPa and poleward of about 40°N (Fig. 7c). Therefore, a large portion of $k = 3$ waves refracts toward the subtropics, instead of propagating into the extratropical stratosphere.

It is worth noting that some portion of $k = 1$ waves also propagate into the subtropical UTLS in DJF (Fig. 7a). This is the reason there is a nonnegligible $k = 1$ forcing in DF spectra at 100 hPa (Fig. 5a). Although $k = 1$ upwelling shows a semiannual cycle as a result of additional wave forcing in JJA, the extratropical $k = 1$ wave is a minor contributor for the observed annual cycle. Also note that $k = 1$ EP flux vectors are heading downward near the tropical tropopause (~15°N and ~100–125 hPa). This feature is consistent with vertical divergence of EP flux observed in $k = 1$ waves (Fig. 5c).

We now discuss potential sources of the $k = 3$ waves focusing on the forcing in the NH subtropics (highlighted by the cross in Fig. 5a). We use the interannual variability of the wavenumber-3 forcing during DJF (over 1979–2012) to quantify forcing mechanisms and find the relevant forcing regions by avoiding spurious relationships from coincident annual cycles. Figure 8 presents interannual variability of the monthly $\langle \bar{w}_{DF_3}^* \rangle$ (dots and error bars). The monthly values show a large interannual spread, and the variability is especially pronounced in the NH winter (DJF), when the upwelling is maximum. This implies that the wave forcing also has a large interannual variability in DJF, from which we can infer its source regions. We first define two indices representing wavenumber-3 activity from the tropics F_{TRO} and extratropics F_{EXT} . Because the $k = 3$ forcing in the NH is largely produced by the horizontal

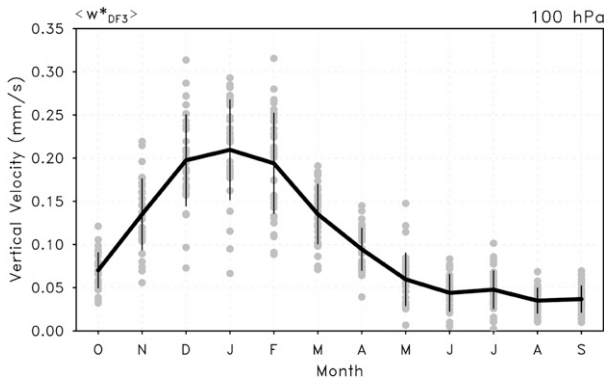


FIG. 8. Monthly $\langle \bar{w}_{DF_3}^* \rangle$ for each year (dots) and its climatology (thick curve). Thin vertical lines denote one standard deviation of the monthly values.

convergence of tropical and extratropical waves, 100-hPa horizontal $k = 3$ EP flux values at their climatological maxima (3.8° and 29.1°N ; points noted by A and B in Fig. 5b) are used for F_{TRO} and F_{EXT} , respectively. Then we regress monthly atmospheric fields (geopotential height, wind, temperature, potential vorticity, and outgoing longwave radiation) to each index. Note that we reversed the sign of the EP flux for F_{EXT} (negative of the horizontal EP flux) in order to make the index positive (i.e., larger F_{EXT}

means stronger equatorward EP flux from the extratropics).

The extratropical component F_{EXT} shows significant relationships with midlatitude regions. The 100-hPa geopotential height regressed onto F_{EXT} (shading in Fig. 9a) shows three high pressure centers, which are collocated with the exit regions of the climatological jet maxima (contours in Fig. 9a). These anomalies have a deep vertical structure, extending from the surface to lower stratosphere levels (~ 70 hPa; not shown). Particularly, the anomalies over the central Pacific and Atlantic Oceans have a westward-tilted structure in the vertical ($\phi'_x T' \sim v' T' > 0$; not shown) and are accompanied by eastward-tilted horizontal wind ($\bar{u}'v' > 0$; vectors in Fig. 9a) at 100 hPa. This structure indicates enhanced upward and equatorward propagation of extratropical waves from the regions. Furthermore, the central Pacific one coincides with a strong dipole of potential vorticity (PV) anomalies (shading in Fig. 9b), implying a reversed PV gradient over the climatologically weak PV-gradient area (northeastern Pacific). Figure 10 shows the likelihood of the PV overturning event over the northeastern Pacific, where the maximum anomalies are found. It shows that the number of potential PV overturning cases increases significantly for months with large F_{EXT} compared to months with small

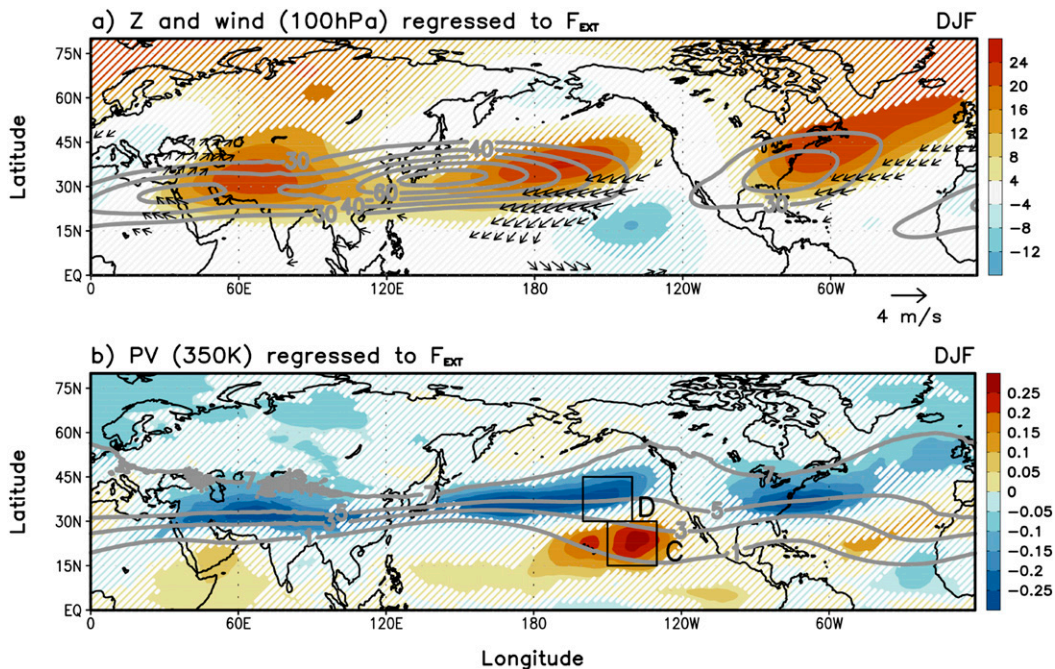


FIG. 9. (a) Geopotential height (m; shading) and wind (vectors) at 100 hPa and (b) potential vorticity at 350 K [PVU; shading] regressed to F_{EXT} during DJF. Climatology of the zonal wind (m s^{-1}) at 200 hPa and potential vorticity (PVU) at 350 K, respectively, are also shown (gray contours). The insignificant area for shading is hatched in white, and only significant wind is shown (based on a Student's t test at the 95% confidence level).

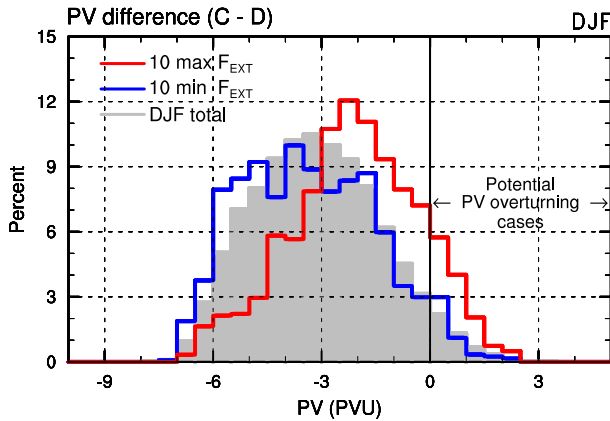


FIG. 10. Frequency distribution of PV difference between two regions defined in Fig. 9b (region C minus region D). Lines indicate the 10 individual months in the DJF season with maximum (red) and minimum (blue) F_{EXT} , and gray shading presents the DJF climatology for 1979–2012. The 6-hourly PV at 350 K is used for the computation. A positive value implies a potential PV overturning event over the northeastern Pacific.

F_{EXT} and climatology. In fact, this mechanism is consistent with that of anticyclonic Rossby wave breaking [LC1 in Thorncroft et al. (1993); see also Postel and Hitchman (1999)], which shears off large PV on the eastern flank of the anticyclone and makes strong wave forcing in the subtropical UTLS. Although it is not clear what condition enhances the PV overturning events, the climatological locations of Rossby wave breaking seem related to the $k = 3$ forcing originated from the NH extratropics during DJF.

Relationships of tropical $k = 3$ forcing F_{TRO} to deep convection and 100-hPa wind speed in the tropics are shown in Fig. 11. The regressed OLR shows a strong minimum (linked to maximum convection) over the western Pacific and maximum over the central eastern Pacific. This is basically an enhanced pattern of climatological convection. In DJF, climatological convection

has three maxima over the western Pacific, South America, and central Africa. This climatological structure could produce a wavenumber-3 component in the convectively driven equatorial waves. The horizontal wind anomaly over the OLR minimum and maximum shows a westward-tilted structure ($\overline{u'v'} < 0$), indicating an enhanced northward propagation of equatorial Rossby waves. Although the regressed OLR and wind do not exactly match the climatological convection structure, they imply that the tropical wave forcing F_{TRO} is related to convection over the western Pacific center, where the climatological maximum is located. Within this pattern the wavenumber-3 structure is also significantly enhanced.

It is worth noting that $k = 1$ and 2 structures are also shown (particularly $k = 2$) in the regressed fields (e.g., OLR in Fig. 11). This implies that $k = 1$ and 2 waves are also enhanced when F_{TRO} ($k = 3$ wave) is strong. It may be natural that strong convective heating in the tropics (e.g., over the western Pacific) forces tropical waves at various scales. However, it is not clearly understood why $k = 1$ and 2 tropical waves cannot make significant forcing at and above 100 hPa. Further study is required.

4. Summary and discussion

The annual cycle in upwelling is the main cause of seasonal variation in many properties in the TTL, including temperature, moisture, and chemical constituents. The upwelling in the TTL, associated with the shallow branch of the BDC, is mechanically forced by tropical and extratropical waves, which dissipate in the subtropics, and it is largely independent of the deep stratospheric circulation (Ueyama et al. 2013; Abalos et al. 2014; Randel and Wu 2015). Thus, our study focuses on wave forcing in the subtropical lower stratosphere, which directly induces tropical upwelling in a shallow vertical depth (70–100 hPa).

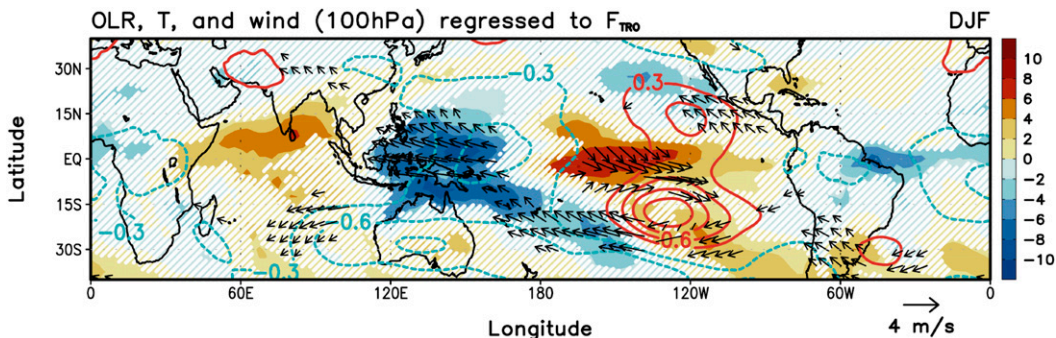


FIG. 11. OLR (shading) and 100-hPa temperature (contours) and wind (vectors) regressed to F_{TRO} . Insignificant OLR is hatched in white, and only significant wind is shown (based on a Student's t test at the 95% confidence level). Temperatures are shown from -0.3 to $+0.3$ K, which is roughly significant at the same confidence level.

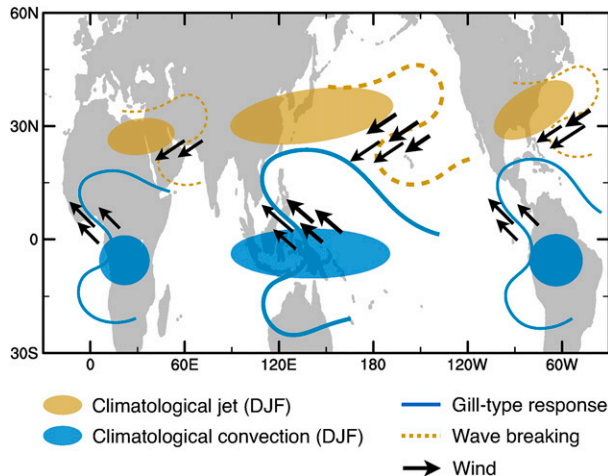


FIG. 12. Schematic diagram for potential sources and forcing mechanisms of climatological $k = 3$ waves in the tropics and extratropics.

The upwelling estimate based on wave forcing and momentum balance (downward control) shows good agreement with the thermodynamic estimate (Fig. 1), and this calculation demonstrates the importance of zonal wavenumber-3 forcing in the annual cycle (Figs. 2–4). Detailed analyses of the wave forcing show a large convergence of the wavenumber-3 component in the NH subtropics at 100 hPa during NH winter (Fig. 5a). These waves are originating both from the NH extratropics and SH tropics. Both tropical and extratropical waves show strong activity at 100 hPa in DJF, but they are almost absent in JJA. A secondary wave forcing in DJF is also found in the SH subtropics over a relatively broader wavenumber band ($k = 2-4$), and this is mostly related to vertical convergence of EP flux likely originating from deep convection in the tropics.

The reason why wavenumber-3 forcing dominates the annual cycle can be partly understood based on its propagation characteristics. Although all extratropical planetary-scale waves ($k = 1-3$) have strong activities during the NH winter, only the $k = 3$ component is trapped in the vertical (based on quasigeostrophic refractive index calculations). A large portion of the $k = 3$ component propagates into the subtropical lower stratosphere and produces an enhanced tropical upwelling in DJF at 100 hPa. This extratropical forcing is particularly noticeable over the eastern Pacific and Atlantic Oceans in the exit regions of the climatological jets. In addition, there is a large $k = 3$ component of wave activity originating in the tropics, likely linked to the climatological structure of deep convection (which has three maxima during DJF). The possible forcing structure is summarized in a schematic diagram (Fig. 12).

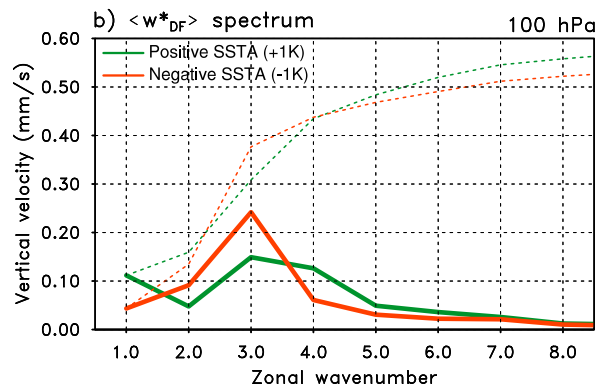
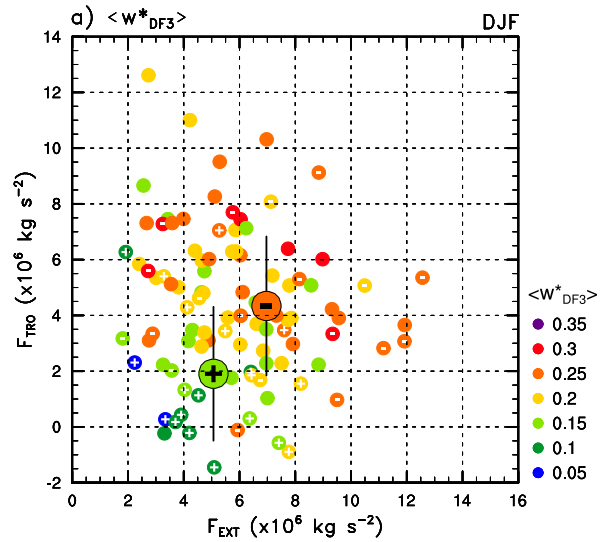


FIG. 13. (a) Monthly $\langle \bar{w}_{DF3}^* \rangle$ (mm s^{-1} ; color) as a function of F_{EXT} and F_{TRO} in December–February. Positive (+) and negative (-) markers indicate months with SST anomalies over the Niño-3.4 region that are larger than +1 K and -1 K, respectively. Big markers indicate their averages, and vertical lines are one standard deviation of their F_{TRO} . (b) Upwelling spectra are as in Fig. 4, but only for the months with positive and negative markers.

The combination of the tropical and extratropical waves, which maximize during boreal winter, produces the dominant annual cycle in wave forcing and associated tropical upwelling near the tropopause.

The relative importance of tropical and extratropical waves in forcing the annual cycle has been the subject of recent research, with conflicting results (e.g., Jucker et al. 2013; Ortland and Alexander 2014). From our analysis, the tropical and extratropical waves have roughly equal contributions to the forcing in the NH subtropics, which is the main cause of the annual cycle in $k = 3$ upwelling. As expected, the amplitude of the $k = 3$ upwelling is sensitive to interannual variations of the separate (tropical and extratropical) forcings (Fig. 13a). We have used the interannual variability to quantify

links to forcing mechanisms in the tropics and extratropics. Enhanced NH extratropical $k = 3$ wave fluxes are related to modulations of the winter storm tracks and wave breaking over the northeastern Pacific and North Atlantic Oceans, but detailed mechanisms in this process are still unclear. For tropical waves, it is worth noting that the regressed OLR and temperature patterns (Fig. 11) are similar to that of La Niña (cold phase of the El Niño–Southern Oscillation). In addition, F_{TRO} and $\langle \bar{w}_{\text{DF}_3}^* \rangle$ are significantly enhanced (diminished) when the sea surface temperature (SST) anomaly over the Niño-3.4 area is colder (warmer) [negative (positive) signs in Fig. 13]. This is largely because of redistribution of wave sources in the tropics. When SST is zonally uniform (with positive SST anomaly over the Niño-3.4 region) the tropical convection (wave source) spread over the tropical band and the wavenumber-3 dominance in the upwelling spectrum becomes weak (Fig. 13b). This demonstrates the influence of tropical convection and equatorial waves on tropical upwelling, but detailed processes need to be further understood.

It is worth noting that total upwelling is stronger with a positive SST anomaly over the Niño-3.4 region compared to that with negative SST anomaly (dotted lines in Fig. 13b). During the positive SST phase, $k = 1$ forcing is as strong as $k = 3$ forcing, and this implies a strong capability of the $k = 1$ wave in driving tropical upwelling. This can be caused by a stronger source of the $k = 1$ wave or change in waveguide (or both). In addition, smaller-scale waves ($k \geq 4$) also show a larger contribution to tropical upwelling during the positive phase. Forcing by resolved synoptic-scale and gravity waves (Calvo et al. 2010) likely increases in the subtropical lower stratosphere during the positive phase; however, this issue needs more comprehensive analysis and understanding.

Acknowledgments. We thank John Albers, Seok-Woo Son, and Rolando Garcia for helpful discussions and comments on this idea and manuscript. We also thank three anonymous reviewers for their constructive comments. This work was partially supported under the NASA GNSS Remote Sensing and Aura Science Teams.

REFERENCES

- Abalos, M., W. J. Randel, and E. Serrano, 2012: Variability in upwelling across the tropical tropopause and correlations with tracers in the lower stratosphere. *Atmos. Chem. Phys.*, **12**, 11 505–11 517, doi:10.5194/acp-12-11505-2012.
- , —, and —, 2014: Dynamical forcing of subseasonal variability in the tropical Brewer–Dobson circulation. *J. Atmos. Sci.*, **71**, 3439–3453, doi:10.1175/JAS-D-13-0366.1.
- , B. Legras, F. Ploeger, and W. J. Randel, 2015: Evaluating the advective Brewer–Dobson circulation in three reanalyses for the period 1979–2012. *J. Geophys. Res. Atmos.*, **120**, 7534–7554, doi:10.1002/2015JD023182.
- Andrews, D. G., J. R. Holton, and C. B. Leovy, 1987: *Middle Atmosphere Dynamics*. International Geophysics Series, Vol. 40, Academic Press, 489 pp.
- Birner, T., and H. Bönisch, 2011: Residual circulation trajectories and transit times into the extratropical lowermost stratosphere. *Atmos. Chem. Phys.*, **11**, 817–827, doi:10.5194/acp-11-817-2011.
- Brewer, A., 1949: Evidence for a world circulation provided by the measurements of helium and water vapour distribution in the stratosphere. *Quart. J. Roy. Meteor. Soc.*, **75**, 351–363, doi:10.1002/qj.49707532603.
- Calvo, N., R. R. Garcia, W. J. Randel, and D. R. Marsh, 2010: Dynamical mechanism for the increase in tropical upwelling in the lowermost tropical stratosphere during warm ENSO events. *J. Atmos. Sci.*, **67**, 2331–2340, doi:10.1175/2010JAS3433.1.
- Chen, G., and L. Sun, 2011: Mechanisms of the tropical upwelling branch of the Brewer–Dobson circulation: The role of extratropical waves. *J. Atmos. Sci.*, **68**, 2878–2892, doi:10.1175/JAS-D-11-044.1.
- Dee, D. P., and Coauthors, 2011: The ERA-Interim reanalysis: Configuration and performance of the data assimilation system. *Quart. J. Roy. Meteor. Soc.*, **137**, 553–597, doi:10.1002/qj.828.
- Dima, I. M., J. M. Wallace, and I. Kraucunas, 2005: Tropical zonal momentum balance in the NCEP reanalyses. *J. Atmos. Sci.*, **62**, 2499–2513, doi:10.1175/JAS3486.1.
- Dobson, G. M. B., 1956: Origin and distribution of the polyatomic molecules in the atmosphere. *Proc. Roy. Soc. London*, **236A**, 187–193, doi:10.1098/rspa.1956.0127.
- ECMWF, 2009: ERA-Interim project. Research Data Archive at the National Center for Atmospheric Research, Computational and Information Systems Laboratory, accessed 30 Mar 2014, doi:10.5065/D6CR5RD9.
- Fueglistaler, S., A. E. Dessler, T. J. Dunkerton, I. Folkins, Q. Fu, and P. W. Mote, 2009: Tropical tropopause layer. *Rev. Geophys.*, **47**, RG1004, doi:10.1029/2008RG000267.
- , P. H. Haynes, and P. M. Forster, 2011: The annual cycle in lower stratospheric temperatures revisited. *Atmos. Chem. Phys.*, **11**, 3701–3711, doi:10.5194/acp-11-3701-2011.
- Garcia, R., 1987: On the mean meridional circulation of the middle atmosphere. *J. Atmos. Sci.*, **44**, 3599–3609, doi:10.1175/1520-0469(1987)044<3599:OTMMCO>2.0.CO;2.
- Garny, H., M. Dameris, W. Randel, G. E. Bodeker, and R. Deckert, 2011: Dynamically forced increase of tropical upwelling in the lower stratosphere. *J. Atmos. Sci.*, **68**, 1214–1233, doi:10.1175/2011JAS3701.1.
- Gille, J., L. Lyjak, and A. Smith, 1987: The global residual mean circulation in the middle atmosphere for the northern winter period. *J. Atmos. Sci.*, **44**, 1437–1452, doi:10.1175/1520-0469(1987)044<1437:TGRMCI>2.0.CO;2.
- Grise, K. M., and D. W. J. Thompson, 2013: On the signatures of equatorial and extratropical wave forcing in tropical tropopause layer temperatures. *J. Atmos. Sci.*, **70**, 1084–1102, doi:10.1175/JAS-D-12-0163.1.
- Haynes, P., M. McIntyre, T. Shepherd, C. Marks, and K. Shine, 1991: On the “downward control” of extratropical diabatic circulations by eddy-induced mean zonal forces. *J. Atmos. Sci.*, **48**, 651–679, doi:10.1175/1520-0469(1991)048<0651:OTCOED>2.0.CO;2.
- Held, I. M., 1983: Stationary and quasi-stationary eddies in the extratropical troposphere: Theory. *Large-scale Dynamical*

- Processes in the Atmosphere*, B. Hoskins and R.P. Pearce, Eds., Academic Press, 127–168.
- Holton, J. R., P. H. Haynes, M. E. McIntyre, A. R. Douglass, R. B. Rood, and L. Pfister, 1995: Stratosphere–troposphere exchange. *Rev. Geophys.*, **33**, 403–439, doi:[10.1029/95RG02097](https://doi.org/10.1029/95RG02097).
- Iwasaki, T., H. Hamada, and K. Miyazaki, 2009: Comparisons of Brewer–Dobson circulations diagnosed from reanalyses. *J. Meteor. Soc. Japan*, **87**, 997–1006, doi:[10.2151/jmsj.87.997](https://doi.org/10.2151/jmsj.87.997).
- Jucker, M., S. Fueglistaler, and G. K. Vallis, 2013: Maintenance of the stratospheric structure in an idealized general circulation model. *J. Atmos. Sci.*, **70**, 3341–3358, doi:[10.1175/JAS-D-12-0305.1](https://doi.org/10.1175/JAS-D-12-0305.1).
- Kerr-Munslow, A. M., and W. A. Norton, 2006: Tropical wave driving of the annual cycle in tropical tropopause temperatures. Part I: ECMWF analyses. *J. Atmos. Sci.*, **63**, 1410–1419, doi:[10.1175/JAS3697.1](https://doi.org/10.1175/JAS3697.1).
- Kiehl, J. T., J. J. Hack, G. B. Bonan, B. A. Boville, B. P. Briegleb, D. L. Williamson, and P. J. Rasch, 1996: Description of the NCAR Community Climate Model (CCM3). National Center for Atmospheric Research Tech. Note NCAR/TN-420+STR, 159 pp., doi:[10.5065/D6FF3Q99](https://doi.org/10.5065/D6FF3Q99).
- Kim, J., and S.-W. Son, 2015: Formation and maintenance of the tropical cold-point tropopause in a dry dynamic-core GCM. *J. Atmos. Sci.*, **72**, 3097–3115, doi:[10.1175/JAS-D-14-0338.1](https://doi.org/10.1175/JAS-D-14-0338.1).
- Liebmann, B., and C. A. Smith, 1996: Description of a complete (interpolated) outgoing longwave radiation dataset. *Bull. Amer. Meteor. Soc.*, **77**, 1275–1277.
- Matsuno, T., 1970: Vertical propagation of stationary planetary waves in the winter Northern Hemisphere. *J. Atmos. Sci.*, **27**, 871–883, doi:[10.1175/1520-0469\(1970\)027<0871:VPOSPW>2.0.CO;2](https://doi.org/10.1175/1520-0469(1970)027<0871:VPOSPW>2.0.CO;2).
- Mote, P., and Coauthors, 1996: An atmospheric tape recorder: The imprint of tropical tropopause temperatures on stratospheric water vapor. *J. Geophys. Res.*, **101**, 3989–4006, doi:[10.1029/95JD03422](https://doi.org/10.1029/95JD03422).
- Norton, W. A., 2006: Tropical wave driving of the annual cycle in tropical tropopause temperatures. Part II: Model results. *J. Atmos. Sci.*, **63**, 1420–1431, doi:[10.1175/JAS3698.1](https://doi.org/10.1175/JAS3698.1).
- Ortland, D. A., and M. J. Alexander, 2014: The residual-mean circulation in the tropical tropopause layer driven by tropical waves. *J. Atmos. Sci.*, **71**, 1305–1322, doi:[10.1175/JAS-D-13-0100.1](https://doi.org/10.1175/JAS-D-13-0100.1).
- Plumb, R. A., 2002: Stratospheric transport. *J. Meteor. Soc. Japan*, **80**, 893–809.
- , and J. Eluszkiewicz, 1999: The Brewer–Dobson circulation: Dynamics of the tropical upwelling. *J. Atmos. Sci.*, **56**, 868–890, doi:[10.1175/1520-0469\(1999\)056<0868:TBDCDO>2.0.CO;2](https://doi.org/10.1175/1520-0469(1999)056<0868:TBDCDO>2.0.CO;2).
- Postel, G., and M. Hitchman, 1999: A climatology of Rossby wave breaking along the subtropical tropopause. *J. Atmos. Sci.*, **56**, 359–373, doi:[10.1175/1520-0469\(1999\)056<0359:ACORWB>2.0.CO;2](https://doi.org/10.1175/1520-0469(1999)056<0359:ACORWB>2.0.CO;2).
- Randel, W. J., and E. J. Jensen, 2013: Physical processes in the tropical tropopause layer and their roles in a changing climate. *Nat. Geosci.*, **6**, 169–176, doi:[10.1038/ngeo1733](https://doi.org/10.1038/ngeo1733).
- , and F. Wu, 2015: Variability of zonal mean tropical temperatures derived from a decade of GPS radio occultation data. *J. Atmos. Sci.*, **72**, 1261–1275, doi:[10.1175/JAS-D-14-0216.1](https://doi.org/10.1175/JAS-D-14-0216.1).
- , R. R. Garcia, and F. Wu, 2002: Time-dependent upwelling in the tropical lower stratosphere estimated from the zonal-mean momentum budget. *J. Atmos. Sci.*, **59**, 2141–2152, doi:[10.1175/1520-0469\(2002\)059<2141:TDUITT>2.0.CO;2](https://doi.org/10.1175/1520-0469(2002)059<2141:TDUITT>2.0.CO;2).
- , —, and —, 2008: Dynamical balances and tropical stratospheric upwelling. *J. Atmos. Sci.*, **65**, 3584–3595, doi:[10.1175/2008JAS2756.1](https://doi.org/10.1175/2008JAS2756.1).
- Reed, R., and C. Vleck, 1969: The annual temperature variation in the lower tropical stratosphere. *J. Atmos. Sci.*, **26**, 163–167, doi:[10.1175/1520-0469\(1969\)026<0163:TATVIT>2.0.CO;2](https://doi.org/10.1175/1520-0469(1969)026<0163:TATVIT>2.0.CO;2).
- Rosenlof, K., 1995: Seasonal cycle of the residual mean meridional circulation in the stratosphere. *J. Geophys. Res.*, **100**, 5173–5191, doi:[10.1029/94JD03122](https://doi.org/10.1029/94JD03122).
- Schoeberl, M. R., B. N. Duncan, R. Douglass, J. Waters, N. Livesey, W. Read, and M. Filipiak, 2006: The carbon monoxide tape recorder. *Geophys. Res. Lett.*, **33**, L12811, doi:[10.1029/2006GL026178](https://doi.org/10.1029/2006GL026178).
- Stolarski, R. S., D. W. Waugh, L. Wang, L. D. Oman, A. R. Douglass, and P. A. Newman, 2014: Seasonal variation of ozone in the tropical lower stratosphere: Southern tropics are different from northern tropics. *J. Geophys. Res. Atmos.*, **119**, 6196–6206, doi:[10.1002/2013JD021294](https://doi.org/10.1002/2013JD021294).
- Taguchi, M., 2009: Wave driving in the tropical lower stratosphere as simulated by WACCM. Part I: Annual cycle. *J. Atmos. Sci.*, **66**, 2029–2043, doi:[10.1175/2009JAS2854.1](https://doi.org/10.1175/2009JAS2854.1).
- Thorncroft, C. D., B. J. Hoskins, and M. E. McIntyre, 1993: Two paradigms of baroclinic-wave life-cycle behaviour. *Quart. J. Roy. Meteor. Soc.*, **119**, 17–55, doi:[10.1002/qj.49711950903](https://doi.org/10.1002/qj.49711950903).
- Trenberth, K., 1991: Climate diagnostics from global analyses: Conservation of mass in ECMWF analyses. *J. Climate*, **4**, 707–722, doi:[10.1175/1520-0442\(1991\)004<0707:CDFGAC>2.0.CO;2](https://doi.org/10.1175/1520-0442(1991)004<0707:CDFGAC>2.0.CO;2).
- Ueyama, R., E. P. Gerber, J. M. Wallace, and D. M. W. Frierson, 2013: The role of high-latitude waves in the intraseasonal to seasonal variability of tropical upwelling in the Brewer–Dobson circulation. *J. Atmos. Sci.*, **70**, 1631–1648, doi:[10.1175/JAS-D-12-0174.1](https://doi.org/10.1175/JAS-D-12-0174.1).
- Yang, Q., Q. Fu, and Y. Hu, 2010: Radiative impacts of clouds in the tropical tropopause layer. *J. Geophys. Res.*, **115**, D00H12, doi:[10.1029/2009JD012393](https://doi.org/10.1029/2009JD012393).
- Yulaeva, E., J. Holton, and J. Wallace, 1994: On the cause of the annual cycle in tropical lower-stratospheric temperatures. *J. Atmos. Sci.*, **51**, 169–169, doi:[10.1175/1520-0469\(1994\)051<0169:OTCOTA>2.0.CO;2](https://doi.org/10.1175/1520-0469(1994)051<0169:OTCOTA>2.0.CO;2).